COMMUNICATION

Check for updates

Non-Fermi liquid to charge-transfer Mott insulator in flat bands of copper-doped lead apatite†

Sun-Woo Kim, [iD] *[a] Kristjan Haule,[b] Gheorghe Lucian Pascut*[c] and Bartomeu Monserrat*[ad]

Copper-doped lead apatite, called LK-99, was initially claimed to be a room temperature superconductor driven by flat electron bands, but was later found to be a wide gap insulator. Despite the lack of room temperature superconductivity, there is growing evidence that LK-99 and related compounds host various strong electron correlation phenomena arising from their flat electron bands. Depending on the copper doping site and crystal structure, LK-99 can exhibit two distinct flat bands crossing the Fermi level in the non-interacting limit: either a single or two entangled flat bands. We explore potential correlated metallic and insulating phases in the flat bands of LK-99 compounds by constructing their correlation phase diagrams, and find both non-Fermi liquid and Mott insulating states. We demonstrate that LK-99 is a charge-transfer Mott insulator driven by strong electron correlations, regardless of the flat band type. We also find that the non-Fermi liquid state in the multi-flat band system exhibits strange metal behaviour, while the corresponding state in the single flat band system exhibits pseudogap behaviour. Our findings align with available experimental observations and provide crucial insights into the correlation phenomenology of LK-99 and related compounds that could arise independently of superconductivity. Overall, our research highlights that LK-99 and related compounds offer a compelling platform for investigating correlation physics in flat band systems.

New concepts

Our work presents a comprehensive theory of the correlation phenomenology arising from flat bands in LK-99 and related compounds. For the first time, we reveal the correlation phase diagrams for two distinct flat bands hosted in two different structures of this compound, encompassing both correlated metallic and insulating states. We demonstrate that the LK-99 compound is a charge-transfer Mott insulator, regardless of the flat band type. We also find that the correlated metallic states are non-Fermi liquids, with characteristics differing significantly between multi and single flat bands. These findings, which arise independently of superconductivity, are consistent with available experimental data. Our results suggest that the correlated states in LK-99 compounds bear similarities to those observed in cuprate superconductors, despite the absence of superconductivity in LK-99 compounds. This comparison provides a valuable opportunity to explore the prerequisites for unconventional superconductivity and deepen our understanding of its enigmatic underlying mechanisms. From a broader materials science perspective, our work offers crucial insights into electron correlation effects in generic flat band materials, including moire and kagome systems, as well as semiconductor systems doped with transition metal or rare-earth atoms that form highly localized states.

1 Introduction

An electronic flat band refers to the energy dispersion of electrons that is confined within a narrow energy window in momentum space, originating from strong localization of electrons in real space. The flat band features a high density of states and quenched kinetic energy, which amplifies electron correlation effects. This makes flat band systems an interesting platform for studying exotic many-body quantum phenomena including the fractional quantum Hall effect,[1,2] ferromagnetism,[3] excitonic insulators,[4] Mott insulators,[5,6] non-Fermi liquid behaviour,[7] and unconventional (potentially high-temperature) superconductivity.[8,9] Archetypal examples of flat band materials include Landau levels in two-dimensional materials under a magnetic field[10,11] and heavy Fermion systems with localized f-electrons.[12] Recent advances in twisted moiré systems[13–16] and kagome materials[17,18] with high tunability have opened a new chapter in the field of flat band materials, stimulating researchers to explore the strongly correlated physics in these materials with the goal of understanding the mechanisms of high-temperature unconventional superconductors and moving toward the dream of room-temperature superconductivity.

[a] Department of Materials Science and Metallurgy, University of Cambridge, 27 Charles Babbage Road, Cambridge CB3 0FS, UK. E-mail: swk38@cam.ac.uk

[b] Center for Materials Theory, Department of Physics & Astronomy, Rutgers University, Piscataway, NJ 08854, USA

[c] MANSiD Research Center and Faculty of Forestry, Stefan Cel Mare University (USV), Suceava 720229, Romania. E-mail: glucian.pascut@usm.ro

[d] Cavendish Laboratory, University of Cambridge, J. J. Thomson Avenue, Cambridge CB3 0HE, UK. E-mail: bm418@cam.ac.uk

† Electronic supplementary information (ESI) available. See DOI: https://doi.org/10.1039/d4mh00971a

The copper-doped lead apatite compound, known as LK-99, was initially claimed to be a room-temperature superconductor.[19,20] Early theoretical studies based on density functional theory (DFT) calculations for a simple model of the LK-99 compound fueled interest by identifying very narrow flat bands crossing the Fermi level, suggesting possible high-temperature flat band superconductivity.[21–24] However, subsequent experimental studies showed that LK-99 is an insulator rather than a superconductor,[25–31] and clarified that the observed resistivity drop originally associated with a superconducting transition was instead caused by a first order structural phase transition of Cu_2S impurities.[32,33] The insulating nature of LK-99 is also supported by DFT calculations including ferromagnetism[34–36] and dynamical mean-field theory calculations without long-range magnetic order.[37–39] Various theoretical estimates of critical superconducting temperatures in (unrealistic) metallic models yielded values significantly lower than room temperature.[40–42]

Despite the lack of high-temperature superconductivity, there is growing evidence that the LK-99 compound represents an interesting class of flat band materials for exploring strongly correlated physics. In a non-interacting limit, it exhibits ideal conditions to explore correlation effects from flat bands, as these flat bands are located exactly at the Fermi level with partial filling and are isolated from other bands, similar to those in twisted moiré systems. What makes the copper-doped lead apatite system particularly interesting is that it hosts two distinct flat bands, either two entangled flat bands or a single flat band crossing the Fermi level. The two flat bands appear in the originally claimed LK-99 structure, while the single flat band appears either at potentially low temperatures or in a different structure with copper doping at a different site.[43] Experimental observations of insulating states without long-range magnetic order in the LK-99 samples[25–29] indeed support the correlated insulating states from flat bands. Moreover, recent experimental

observations of correlated metallic phases with non-Fermi liquid (NFL) behaviour in sulfur-doped LK-99 samples[44] further substantiate the interesting strong correlation physics.

In this work, we study correlated metallic and insulating phases in two distinct flat band systems in copper-doped lead apatite and construct their correlation phase diagrams. We demonstrate the LK-99 compound is a charge-transfer Mott insulator with a wide gap due to strong electron correlations in both flat band systems. Additionally, we reveal how the correlated Mott insulating state evolves from correlated metallic states, specifically NFL states, as the electron correlation strength increases. Furthermore, we discover that the NFL states have drastically different characteristics in the two flat band systems. Specifically, the NFL state in the two flat bands system exhibits strange metal behaviour while the NFL state in the single flat band system exhibits pseudogap behaviour. Our findings of both correlated metallic and insulating states are consistent with available experimental observations for both LK-99 and LK-99 related compounds. Our work provides crucial insights into the correlation phenomenology in non-superconducting LK-99 compounds, highlighting LK-99 as an interesting flat band material for studying strongly correlated physics arising from flat bands.

2 Results

The parent lead apatite compound, $Pb_{10}(PO_4)_6O$, crystallizes in a hexagonal lattice with space group $P3$. There are two symmetrically distinct lead sites, labelled Pb(1) and Pb(2) (see Fig. 1a), and previous experiments observed that copper can be doped at both sites.[29,45] In this work, we focus on copper doping at the Pb(1) site only, motivated by claims associating this particular doping site with room-temperature superconductivity,[19,20] and also by its intriguing electronic and structural properties, which
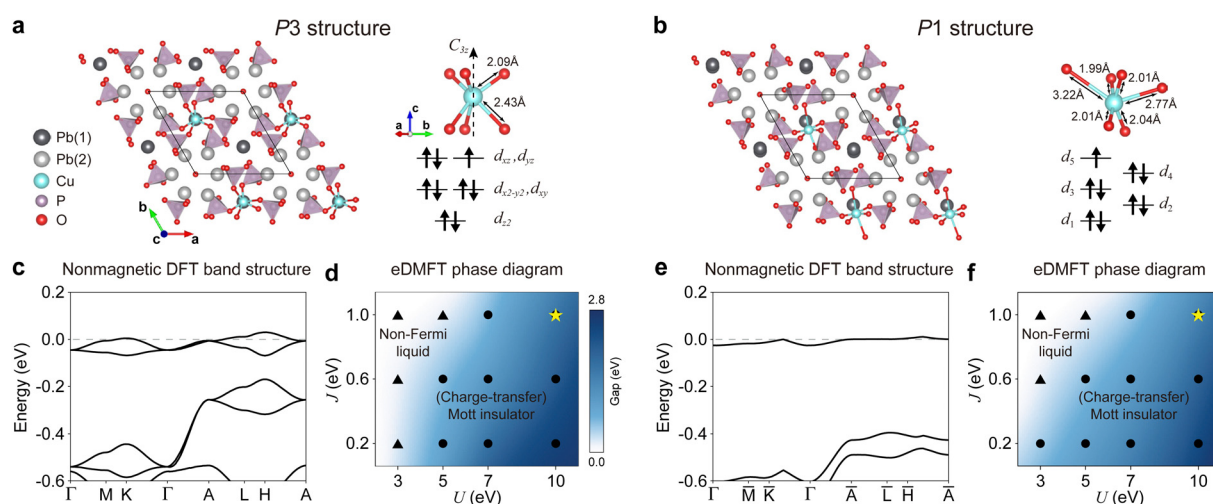

Fig. 1 Crystal structures, electronic structures, and correlation phase diagrams of copper-doped lead apatite. (a) and (b) Crystal structures of $Pb_9Cu(PO_4)_6O$ with a $P3$ space group and b $P1$ space group. (c) DFT band structure for the $P3$ structure. (d) eDMFT phase diagram in the Hubbard U and Hund's coupling J parameter spaces for the $P3$ structure. (e) DFT band structure for the $P1$ structure. (f) eDMFT phase diagram in the U and J parameter spaces for the $P1$ structure. In (d) and (f), the color bar indicates the Mott gap near the Fermi level. Triangles represent metallic states, while circles represent insulating states. The star indicates the constrained eDMFT values of U and J.

include two entangled narrow energy bands crossing the Fermi level at the DFT level without a magnetic order and a possible structural phase transition at low temperatures to a low-symmetry structure, as predicted by theory.[43,46] It is also worth noting that the electronic structure of the low-symmetry phase with the Pb(1) doping is similar to the electronic structure of the Pb(2) doped phase,[43] suggesting that the study of the Pb(1) case allows us to encompass a broad range of correlation phenomenology in the copper-doped lead apatite system.

Copper doping at the Pb(1) site results in a structure that preserves the $P3$ space group of the parent compound (Fig. 1a; see also ESI,† Note S1 for a detailed comparison between the calculated structure and experimental data). A previous study demonstrated that this structure is stable at room temperature due to anharmonic phonon–phonon interactions, and that at lower temperature it may undergo a structural phase transition to a low-symmetry structure with the $P1$ space group[43] (Fig. 1b). In the $P3$ structure, the oxygen octahedra surrounding the copper atom exhibit C_{3z} symmetry, resulting in two different Cu–O bond lengths of 2.09 Å and 2.43 Å. In contrast, in the $P1$ structure, this symmetry is broken, leading to significantly different Cu–O bond lengths ranging from 1.99 Å to 3.22 Å.

In the local atomic picture, the oxygen octahedral crystal field in the $P3$ structure leads to three different energy sub-spaces for the copper d orbitals: a d_{z^2} orbital, two degenerate $d_{x^2-y^2}$ and d_{xy} orbitals, and two degenerate d_{xz}, and d_{yz} orbitals; arranged in ascending order of energy (Fig. 1a). In the $P1$ structure, the degeneracy of copper d orbitals is completely lifted and we label the five d orbitals as d_1, d_2, ..., and d_5 in ascending order of energy (Fig. 1b). The copper atom has a d^9 configuration, and electron counting leads to fully occupied d_{z^2}, $d_{x^2-y^2}$, and d_{xy} orbitals and a partial occupation of the degenerate d_{xz} and d_{yz} orbitals in the $P3$ structure. For the $P1$ structure, electron counting leads to four d orbitals being fully filled, and the higher energy d_5 orbital being only half-filled.

The local atomic picture is robust, resulting in DFT electronic structures that exhibit narrow flat bands near the Fermi level. This is due to the large distance between copper atoms in both structures (at least 7.4 Å), leading to well-localized copper d orbitals. These atomically localized flat bands are similar to those found in 4f states in heavy Fermion systems,[12] and are distinct from flat bands caused by destructive interference effects in specific lattice structures such as Lieb and kagome lattices.[16] The electronic band structure of the $P3$ structure hosts two flat bands with 3/2 filling crossing the Fermi level (Fig. 1c), while that of the $P1$ structure features a half-filled single flat band at the Fermi level (Fig. 1e). We emphasize that the above description, based on simple electron counting and DFT band structures, does not rigorously consider electron correlations. Below, we discuss the importance of the Hubbard U and Hund's coupling J in determining the actual occupancy of the copper d orbitals and the resulting correlated electronic structures in copper-doped lead apatite.

We explore the role of electron correlations on the electronic structure of copper-doped lead apatite by investigating the DFT + embedded dynamical mean-field theory (eDMFT) phase

diagrams of the two structures in the space spanned by the Hubbard U and Hund's coupling J parameters (see Fig. 1d and f). The phase diagrams of the two structures exhibit striking similarities. At small U and large J values both structures are metallic, with a slightly greater metallic region observed for the $P3$ structure. As the Hubbard U increases, both systems become insulators, with their gaps increasing accordingly. Increasing the Hund's coupling J has the opposite effect to that of Hubbard U by enhancing metallicity. Although, in general, J compensates for the effect of U, it is rather unexpected that small changes in J values significantly affect the electronic properties, driving a metal-to-insulator transition as shown in the phase diagrams. This is notable because Hund's coupling J is typically crucial in multiorbital (or d^8) systems, rather than in this one-hole d^9 system like the cuprate superconductor.[47–49] The insulating states are paramagnetic (charge-transfer) Mott insulators while the metallic states are non-Fermi liquids, which will be clarified below.

The *ab initio* constrained eDMFT values of U and J are estimated as $U = 10$ eV and $J = 1$ eV. At these values for U and J, our theory predicts that both structures are wide gap Mott insulators with a gap of 1.8 eV for the $P3$ structure and of 1.6 eV for the $P1$ structure (star in the phase diagrams in Fig. 1d and f, and see also Fig. 2 for detailed electronic structures). Our results are consistent with experimental reports showing highly insulating behaviour,[25–31] as well as with previous theoretical studies that also included electron correlations effects.[37–39] In contrast to previous DFT results,[34–36] we do not need to assume a ferromagnetic state to obtain an insulating phase. Moreover, compared to previous Wannier-based DMFT studies,[37–39] our predicted Mott gap is larger.

In what follows, we explore in detail both metallic and insulating states. We propose copper-doped lead apatite as a prototypical example of a wide gap insulator with transition metal atom doping, where dopants form localized impurity-like states, exhibiting narrow flat bands. We anticipate that different dopants or external perturbations, such as hydrostatic pressure or strain, which can be used to suppress electron correlations, would enable the exploration of our proposed U–J phase diagram. Later, we will indeed discuss the accessibility of metallic states depicted in our phase diagram, as examined in recent experiments involving sulfur-doped LK-99 samples.[44]

We present representative correlated electronic structures of metallic and insulating states for the two structures at room temperature in Fig. 2. For metallic states ($U = 3$ and $J = 1$ eV; see Fig. 2a and b), the electronic structures of both structures show significant spectral weight near the Fermi level, primarily composed of copper and oxygen orbitals. The density of states (DOS) for the $P3$ structure exhibits a single sharp peak, whereas the DOS for the $P1$ structure displays two peaks. The relevant copper d orbitals for these states are the d_{xz} and d_{yz} orbitals for the $P3$ structure and the d_5 orbital for the $P1$ structure, consistent with the local atomic picture and DFT band structures discussed earlier. However, the eDMFT electronic structures of the metallic phases are markedly different from those obtained from DFT in Fig. 1c and e (see also ESI† Note S2 for a
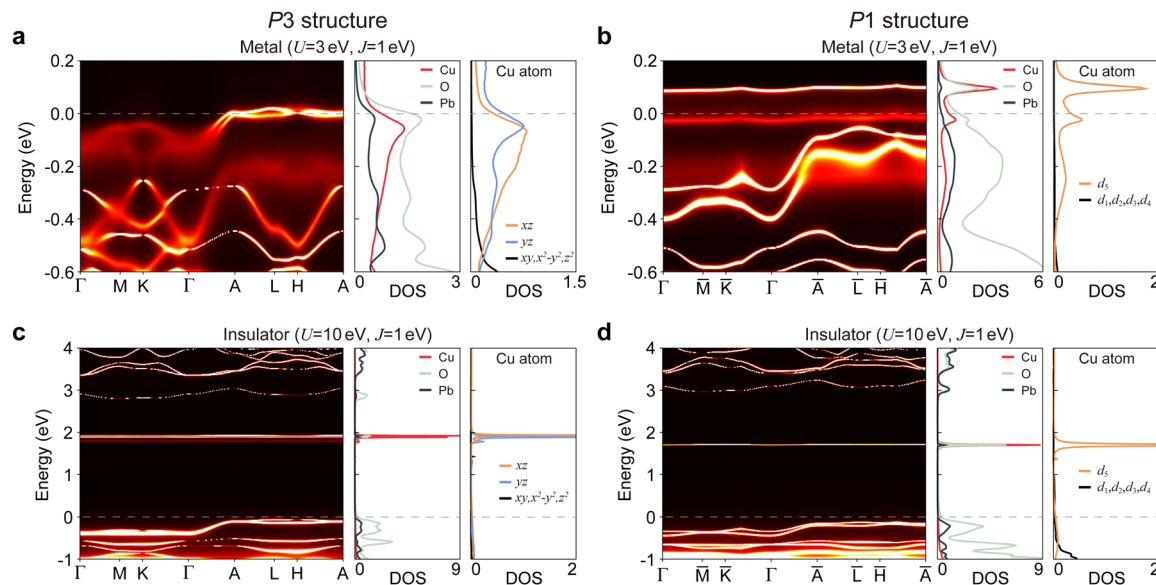
Fig. 2 Metallic and insulating electronic structures of copper-doped lead apatite. (a) and (b) Spectral function and density of states (DOS) for metallic states in the a $P3$ structure and b $P1$ structure. U = 3 eV and J = 1 eV are used. (c) and (d) Spectral function and DOS for insulating states in the c $P3$ structure and d $P1$ structure. U = 10 eV and J = 1 eV are used. All data are obtained at a temperature of 300 K.

broader energy window comparison). As discussed below in detail, this difference is caused by the fact that these are highly correlated metallic states exhibiting non-Fermi liquid behaviour, as hinted by the incoherent nature of the spectral functions around the Fermi level. We also note that the spectral functions of the two structures are distinct near the Fermi level. The $P3$ structure exhibits a mixture of incoherent and coherent spectral features depending on the Brillouin zone (BZ) region, with particularly coherent states at the Fermi level. By contrast, the $P1$ structure exhibits highly incoherent states at the Fermi level across the whole BZ, showing a pseudo-gap like electronic structure.

For insulating states (U = 10 and J = 1 eV; see Fig. 2c and d), the copper orbitals undergo significant changes compared to the metallic states, forming a charge-transfer Mott gap of 1.8 and 1.6 eV for the $P3$ and $P1$ structures, respectively. The relevant copper states comprise the flat lowest unoccupied states, characterized by a very narrow bandwidth. These unoccupied flat bands are located within the fundamental bulk gap of the parent lead aptite compound (without copper doping) formed by lead and oxygen states, with a value of 2.7 eV for the $P3$ structure and of 2.9 eV for the $P1$ structure. The bulk gap of the $P3$ structure is almost identical to that of the parent lead apatite bulk gap, and this gap becomes larger in the $P1$ structure due to the distortion of lead and oxygen atoms. The formation and evolution of the copper flat bands are detailed below. It is noteworthy that eDMFT electronic structures of the insulating phases are also different from DFT (see ESI† Note S2), as the eDMFT calculations are performed for paramagnetic states, rather than the long-range ferromagnetic states required in DFT-level calculations to open a gap.

Fig. 3 shows the evolution of the DOS of copper correlated d orbitals as a function of U and J. With fixed J = 1 eV, increasing

U leads to the formation of a sharp narrow peak composed of d_{xz} and d_{yz} orbitals for the $P3$ structure as it undergoes a phase transition from a metallic to an insulating state (Fig. 3a). It is noteworthy that at U = 5 eV, the $P3$ structure remains metallic with a pseudo-gap-like DOS. This pseudo-gap-like feature also exists in the metallic state with the peak of the d_5 orbital of the $P1$ structure at U = 3 and U = 5 eV (with J = 1 eV; Fig. 3b). As a result, at U = 10 eV (with J = 1 eV), both structures exhibit a sharp peak composed of the correlated d orbitals within the fundamental bulk gap formed by oxygen and lead orbitals. This sharp peak remains robust against temperature changes from 100 K to 1900 K, with small shifts in its position within the fundamental gap depending on temperature (see ESI† Note S3).
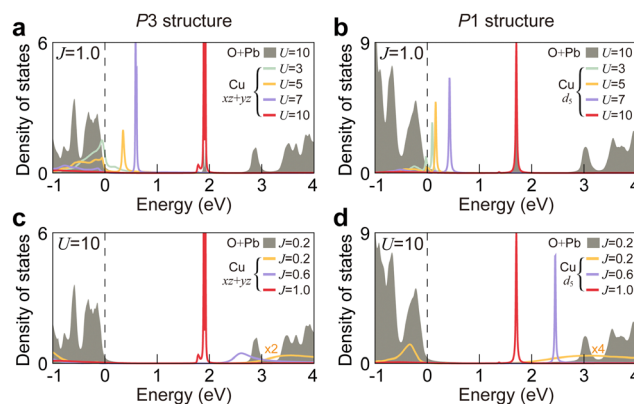

Fig. 3 Influences of Hubbard U and Hund's coupling J on copper d orbital states. (a) and (b) DOS of copper d orbitals for the a $P3$ structure and b $P1$ structure as a function of Hubbard U. J = 1.0 eV is used. (c) and (d) DOS of copper d orbitals for the c $P3$ structure and d $P1$ structure as a function of Hund's coupling J. U = 10 eV is used. For comparison, the DOS of oxygen and lead states are shown in shaded grey.

When the J decreases (so the effective U increases), the sharp peak further moves towards the upper bulk states (Fig. 3c and d). If the peak overlaps with the bulk states, it broadens and is eventually suppressed due to the hybridization with the bulk states.

We further characterize the metallic and insulating states by examining their self-energy in detail (Fig. 4). Our analysis reveals that both structures exhibit non-Fermi liquid (NFL) behaviour in their metallic states, with distinct characteristics between the two structures hinted at above in the discussion of their electronic structures in Fig. 2. The NFL nature is identified by the low-frequency behaviour of the imaginary part of the local Matsubara self-energy, $Im\Sigma(i\omega_n)$: it deviates from linear behaviour at low temperature as $Im\Sigma(i\omega_n) \sim A(i\omega_n)^{\alpha}$ with $\alpha \neq 1$ and its intercept $Im\Sigma(i\omega_n \to 0^+)$ shows a non-quadratic temperature dependence. We also confirm the NFL nature using the first Matsubara frequency rule (see ESI† Note S4). The intercept and the slope A represent the scattering rate and the quantity directly associated with quasiparticle mass renormalization, respectively, in Landau Fermi liquid theory. Although the quasiparticle concept is generally lost in NFLs, it remains meaningful in certain types of NFLs with a negative slope $A < 0$ of $Im\Sigma(i\omega_n)$, where the negative slope is used as a measure of mass enhancement due to electron correlations. In our system, this is the case for the $P3$ structure (left panel in Fig. 4a). We refer to the NFL state in the $P3$ structure as a bad-metallic NFL, since it still shows metallic behaviour of the scattering rate, *i.e.*, increasing as a function of T, notably with a linear dependence (strange metal behaviour) below 500 K, and saturated at higher temperature (Fig. 4c). On the other hand, the NFL state of the $P1$ structure exhibits markedly contrasting behaviour, featuring a positive slope $A > 0$ of $Im\Sigma(i\omega_n)$ with negligible temperature dependence (left panel in Fig. 4b). The

positive slope indicates a highly incoherent state devoid of the quasiparticle concept. The scattering rate of the $P1$ structure shows nonmonotonic temperature dependence, particularly a decreasing behaviour with increasing T (Fig. 4e). The decreasing behaviour is also reported in the NFL state in the Lieb lattice with a flat band[50] and in the single band Hubbard model at half filling.[51] We refer to this as the pseudogap NFL. The pseudogap NFL in the $P1$ structure is a more correlated state than the bad-metallic NFL in the $P3$ structure as the $Im\Sigma(i\omega_n)$ of the $P3$ structure exhibits similar pseudogap NFL behaviour when J is reduced (see ESI† Note S5). This suggests that the two entangled energy bands in the $P3$ structure result in a metallic state with reduced correlations at identical U and J values.

For the insulating states, both structures are characterized as charge-transfer Mott insulators. The low-frequency behaviour of the imaginary part of the local Matsubara self-energy $Im\Sigma(i\omega_n)$ exhibits similar behaviour in both structures: it extrapolates to zero at zero imaginary frequency, as there are no electrons to scatter, which is expected for insulating states, and it shows negligible temperature dependence (right panels in Fig. 4a and b). The real and imaginary parts of the self energy on the real axis exhibit a pole within the gap for both structures (Fig. 4d and f), indicating an electron-correlation-driven Mott gap. Considering the atom-projected DOS of both structures (Fig. 2c, d and 3), they are characterized as charge-transfer type insulators, where the charge transfer occurs between oxygen p orbitals and copper d orbitals, forming the gap with valence bands composed mainly of oxygen p orbitals and conduction bands composed mainly of copper d orbitals. As a result, we refer to the insulating states of both structures as charge-transfer Mott insulators.

Finally, we analyze the occupancy of copper d orbitals and their microstates as the interaction parameters U and J change
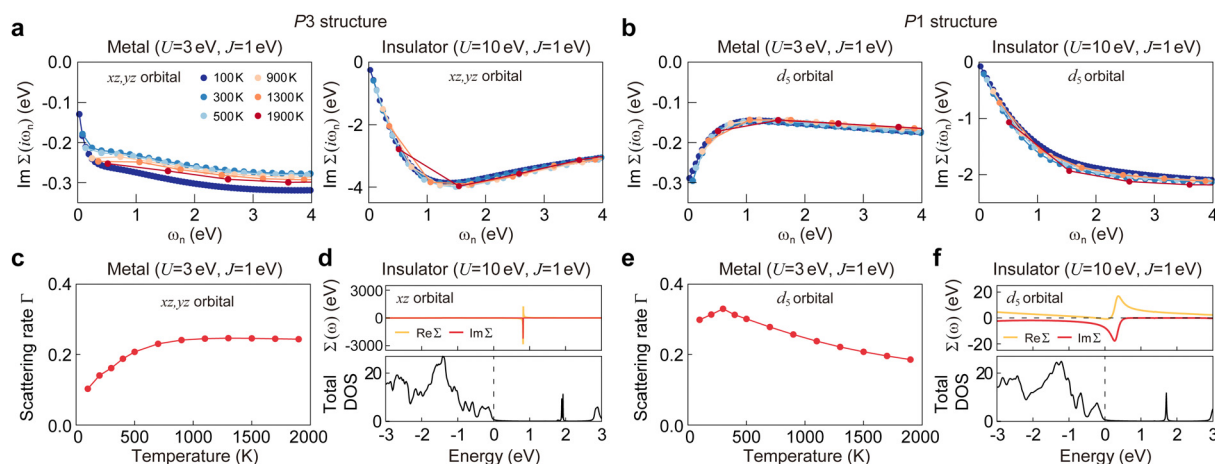

Fig. 4 Characterization of non-Fermi liquid and charge-transfer Mott insulator. (a) and (b) Temperature evolution of the imaginary part of the self energy on the imaginary axis, $Im\Sigma(i\omega_n)$, for a the $P3$ structure and b the $P1$ structure. We display $Im\Sigma(i\omega_n)$ for the averaged d_{xz} and d_{yz} orbitals in the $P3$ structure, and the d_5 orbital in the $P1$ structure, respectively (see ESI† Note S5 for the self-energy of other orbitals). (c) Scattering rate of the metallic state of the $P3$ structure as a function of temperature. The scattering rate is averaged over the d_{xz} and d_{yz} orbitals. (d) Self energy on the real axis and total DOS of the insulating state of the $P3$ structure. (e) Scattering rate of the metallic state of the $P1$ structure as a function of temperature. In (c) and (e), the scattering rate $\Gamma \sim -Im\Sigma(i0^+)$ is obtained using a linear fit over the first two Matsubara frequencies. (f) Self energy on the real axis and total DOS of the insulating state of the $P1$ structure.
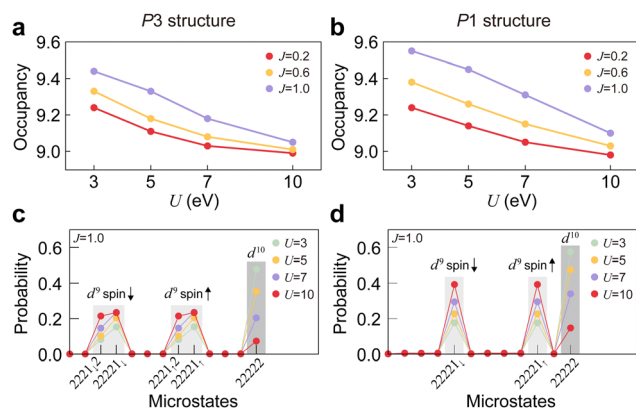
Fig. 5 Occupancy of copper d orbitals and their valence histogram. (a) and (b) Occupancy of copper d orbitals as a function of U and J for a the $P3$ structure and b the $P1$ structure. (c) and (d) Valence histogram as a function of U ($J = 1$ eV) for c the $P3$ structure and d the $P1$ structure. $22221_\uparrow$ refers to the d^9 electron configuration of copper, where the the first four orbitals are fully occupied (denoted as 2), and the fifth orbital is half occupied by a spin-up electron (denoted as $1_\uparrow$). The orbital sequence is $\{d_{z^2}, d_{x^2-y^2}, d_{xy}, d_{xz}, d_{yz}\}$ for the $P3$ structure and $\{d_1, d_2, d_3, d_4, d_5\}$ for the $P1$ structure.

(Fig. 5). At lower interaction parameter values ($U = 3$ and $J = 1$ eV), corresponding to the NFL states discussed above, the calculated copper d occupancies are 9.44 and 9.55 for the $P3$ and $P1$ structures, respectively, due to a high probability of d^{10} configurations. These occupancies in NFL states deviate from a d^9 configuration typically assumed in general model studies based on the Cu^{2+} valence state derived from the stoichiometry. The occupancy of copper d orbitals decreases as U increases (J decreases) for both structures, becoming 9.05 and 9.10 in the charge-transfer Mott insulator regime (at $U = 10$ and $J = 1$ eV) for the $P3$ and $P1$ structures, respectively, owing to the increasing probability of the d^9 configuration. It is noteworthy that for the $P3$ structure, the probabilities of d_{xz} and d_{yz} orbitals become identical only when U is sufficiently large. This analysis provides important insights for future studies on NFL states as well as charge-transfer Mott insulating states in these prototypical flat band compounds.

3 Discussion

Our proposed correlation phase diagrams in two distinct flat band systems encompass a broad correlation phenomenology, ranging from correlated metallic to correlated insulating states arising from Mott physics, with direct relevance to experimental observations in LK-99 and related compounds. For the insulating states found in both flat band systems, our theory predicts a correlated Mott insulating phase with paramagnetism arising from local magnetic moments. This calculated insulating phase is consistent with the highly insulating nature of some LK-99 samples exhibiting paramagnetic behaviour.[25,26] For the newly revealed NFL states, particularly the NFL state in the two entangled flat bands in the $P3$ structure, the calculated temperature-dependent scattering rate shows a remarkable

qualitative similarity to the resistivity behaviour of correlated metallic states reported in sulfur-doped LK-99 compounds[44]: T-linear behaviour from low temperatures (starting around 20 K; depending on the samples) and saturation above 300 K. Our theory indicates that the T-linear resistivity has an anomalous origin from electron correlations rather than the conventional electron–phonon coupling origin. We attribute the emergence of this NFL state to reduced effective electron correlations. We note that our theory is not compatible with the diamagnetic behaviour in some LK-99 and doped LK-99 samples, which requires further study.

The anomalous T-linear resistivity is a hallmark of the strange metal phase, which is known as the parent correlated metallic state of the superconducting state in high-temperature cuprates and other unconventional superconductors.[52] In this context, recent experimental work[44] argued for possible superconductivity in LK-99 and related compounds due to the observation of strange metal behaviour in sulfur-doped LK-99, analogous to other unconventional superconductors, as well as a strong diamagnetic response, reigniting the claim of the existence of superconductivity in this system.[44,53,54] Our calculations suggest that such strange metal behaviour could arise from the strong electron correlations associated with the flat bands in the system. However, the existence of a strange metal phase does not guarantee the presence of superconductivity, as strange metal phases have been observed in both superconducting[55–58] and non-superconducting[18,59] materials. Moreover, we note that the spin exchange in the LK-99 compound is extremely small compared to that in cuprate supercondutors, as our eDMFT calculations show that the antiferromagnetic state is unstable even at 100 K. This small spin exchange precludes the possibility of high-temperature unconventional superconductivity similar to that observed in cuprates. Our results contribute to settling the on-going discussion regarding the original claim of room temperature superconductivity. Our work suggests that LK-99 compounds under doping or pressure represent additional intriguing strange metal candidates. Expanding the range of strange metal materials provides a valuable opportunity to explore the prerequisites for unconventional superconductivity and gain a deeper understanding of its enigmatic underlying mechanisms.

4 Conclusions

Our research highlights that LK-99 and related compounds provide a compelling platform for investigating correlation physics in both multi- and single-flat band systems. Specifically, the multi-flat band system exhibits distinctly different correlated metallic phases compared to the single-flat band system, offering valuable insights into correlated phenomena within flat band materials. This serves as a pertinent material example amidst ongoing research into correlation effects in moiré and kagome materials, and could potentially apply to generic semiconductor systems doped with transition metal or rare-earth atoms that form highly localized states. The correlation phase

diagrams we calculate, encompassing Mott insulators and non-Fermi liquid metallic states, exhibit similarities to those observed in cuprate superconductors despite the absence of room-temperature superconductivity in LK-99 compounds. This comparison prompts future experimental and theoretical studies to explore these intriguing parallels further.

5 Methods

5.1 Density functional theory (DFT) calculations

We perform DFT calculations using the full-potential linearized augmented plane wave (FP-LAPW) method as implemented in the wien2k code.[60] For the exchange–correlation energy, we use the generalized-gradient approximation functional of Perdew–Burke–Ernzerhof (PBE).[61] For Brillouin zone integrations, we use the tetrahedron integration method with 3000 and 1160 k-points in the full Brillouin zone, corresponding to $13 \times 13 \times 15$ and $11 \times 9 \times 10$ k-grids for the $P3$ structure and the $P1$ structure, respectively. We use self-consistency cycle stopping criteria of 5×10^{-5} Ry for the energy and 5×10^{-5} e for the charge. The radii (R) of the muffin-tin (MT) spheres are taken to be 1.97, 2.22, 1.41 and 1.34 Bohr for Cu, Pb, O and P atoms, respectively. $R_{MT} \times K_{max}$ is set to 5.5 (confirming that using 7 yields the same results), where K_{max} is the cutoff value of the modulus of the reciprocal lattice vectors and R_{MT} is the smallest MT radius. We optimise the lattice parameters for both the $P3$ and the $P1$ structures and the internal coordinates are optimised until all forces are below 0.5 mRy bohr^{-1}.

5.2 DFT + embedded dynamical mean-field theory (DFT + eDMFT) calculations

We perform fully self-consistent DFT + eDMFT calculations. The iterations stop after full convergence of the charge density, the impurity level, the chemical potential, the self-energy, and the lattice and impurity Greens functions. Double counting between the DFT and DMFT correlations is treated within an exact double-counting scheme.[62] The fully rotational invariant form of the Coulomb repulsion[63] is employed, as it is found to be essential for accurately describing the copper-doped lead apatite compounds due to their low symmetry structures. We use a large hybridization window of ±10 eV. For the DMFT projectors, we choose quasi-atomic localized orbitals. The radial part is determined by solving the Schrödinger equation within the muffin-tin sphere, with the linearized energy at the Fermi level, and the angular dependence provided by spherical harmonics. For the quantum impurity problem (Cu-3d electrons), we use a version of the continuous time quantum Monte Carlo (CTQMC) impurity solver[64,65] with a total of $512 \times 20 \times 10^6$ Monte Carlo steps. The position of the chemical potential is allowed to vary during the self-consistent calculations. Analytic continuation from the imaginary to real frequency axis is conducted using the maximum entropy method.

Author contributions

S.-W. K., K. H., G. L. P. and B. M. conceived the study. S.-W. K., G. L. P., and B. M. planned and supervised the research. S.-W. K. performed the DFT calculations, S.-W. K., K. H., and G. L. P. performed the eDMFT calculations. S.-W. K. and B. M. wrote the manuscript with input from all authors.

Data availability

The authors confirm that the data supporting the findings of this study are available within the article and the ESI.†

Conflicts of interest

There are no conflicts of interest to declare.

Acknowledgements

References

1 D. C. Tsui, H. L. Stormer and A. C. Gossard, Two-dimensional magnetotransport in the extreme quantum limit, *Phys. Rev. Lett.*, 1982, **48**, 1559–1562.

2 E. Tang, J.-W. Mei and X.-G. Wen, High-temperature fractional quantum hall states, *Phys. Rev. Lett.*, 2011, **106**, 236802.

3 A. Mielke, Ferromagnetic ground states for the Hubbard model on line graphs, *J. Phys. A: Math. Gen.*, 1991, **24**, L73.

4 G. Sethi, Y. Zhou, L. Zhu, L. Yang and F. Liu, Flat-band-enabled triplet excitonic insulator in a diatomic kagome lattice, *Phys. Rev. Lett.*, 2021, **126**, 196403.

5 J. Hubbard, Electron correlations in narrow energy bands, *Proc. - R. Soc. Edinburgh, Sect. A: Math. Phys. Sci.*, 1963, **276**, 238–257.

6 N. F. Mott, Metal-insulator transition, *Rev. Mod. Phys.*, 1968, **40**, 677–683.

7 P. Kumar, T. I. Vanhala and P. Törmä, Magnetization, *d*-wave superconductivity, and non-Fermi-liquid behavior in a crossover from dispersive to flat bands, *Phys. Rev. B*, 2019, **100**, 125141.

8 R. Micnas, J. Ranninger and S. Robaszkiewicz, Superconductivity in narrow-band systems with local nonretarded attractive interactions, *Rev. Mod. Phys.*, 1990, **62**, 113–171.

9 H. Aoki, Theoretical possibilities for flat band superconductivity, *J. Supercond. Novel Magn.*, 2020, **33**, 2341–2346.

10 L. Landau, Diamagnetismus der metalle, *Z. Phys.*, 1930, **64**, 629–637.

11 K. v Klitzing, G. Dorda and M. Pepper, New method for high-accuracy determination of the fine-structure constant based on quantized hall resistance, *Phys. Rev. Lett.*, 1980, **45**, 494–497.

12 Q. Si and F. Steglich, Heavy Fermions and quantum phase transitions, *Science*, 2010, **329**, 1161–1166.

13 Y. Cao, *et al.*, Unconventional superconductivity in magic-angle graphene superlattices, *Nature*, 2018, **556**, 43–50.

14 Y. Cao, *et al.*, Correlated insulator behaviour at half-filling in magic-angle graphene superlattices, *Nature*, 2018, **556**, 80–84.

15 L. Balents, C. R. Dean, D. K. Efetov and A. F. Young, Superconductivity and strong correlations in moiré flat bands, *Nat. Phys.*, 2020, **16**, 725–733.

16 J. G. Checkelsky, B. A. Bernevig, P. Coleman, Q. Si and S. Paschen, Flat bands, strange metals and the kondo effect, *Nat. Rev. Mater.*, 2024, **9**, 509–526.

17 M. Kang, *et al.*, Topological flat bands in frustrated kagome lattice CoSn, *Nat. Commun.*, 2020, **11**, 4004.

18 L. Ye, *et al.*, Hopping frustration-induced flat band and strange metallicity in a kagome metal, *Nat. Phys.*, 2024, **20**, 610–614.

19 S. Lee, J.-H. Kim and Y.-W. Kwon *The firs room-temperature ambient-pressure superconductor*, *arXiv*, 2023, preprint, arXiv:2307.12008.

20 S. Lee *et al.* Superconductor $Pb_{10-x}Cu_x(PO_4)O$ showing levitation at room temperature and atmospheric pressure and mechanism, *arXiv*, 2023, preprint, arXiv:2307.12037.

21 S. M. Griffin *Origin of correlated isolated flat bands in copper-substituted lead phosphate apatite*, *arXiv*, 2023, preprint, arXiv:2307.16892.

22 L. Si and K. Held, Electronic structure of the putative room-temperature superconductor $Pb_9 Cu(PO_4)_6 O$, *Phys. Rev. B*, 2023, **108**, L121110.

23 J. Lai, J. Li, P. Liu, Y. Sun and X.-Q. Chen, First-principles study on the electronic structure of $Pb_{10-x}Cu_x(PO_4)_6 O$ ($x = 0,1$), *J. Mater. Sci. Technol.*, 2024, **171**, 66–70.

24 R. Kurleto *et al.* Pb-apatite framework as a generator of novel flat-band CuO based physics, including possible room temperature superconductivity, *arXiv*, 2023, preprint, arXiv:2308.00698.

25 L. Liu, *et al.*, Semiconducting transport in $Pb_{10-x}Cu_x(PO_4)_6 O$ sintered from $Pb_2 SO_5$ and $Cu_3 P$, *Adv. Funct. Mater.*, 2023, **33**, 2308938.

26 K. Guo, Y. Li and S. Jia, Ferromagnetic half levitation of LK-99-like synthetic samples, *Sci. China: Phys., Mech. Astron.*, 2023, **66**, 107411.

27 K. Kumar, N. Kumar Karn, Y. Kumar and V. Awana, Absence of superconductivity in LK-99 at ambient conditions, *ACS Omega*, 2023, **8**, 41737–41743.

28 C. Liu, *et al.*, Phases and magnetism at microscale in compounds containing nominal $Pb_{10-x}Cu_x(PO_4)_6 O$, *Phys. Rev. Mater.*, 2023, **7**, 084804.

29 P. Puphal, *et al.*, Single crystal synthesis, structure, and magnetism of $Pb_{10-x}Cu_x(PO_4)_6 O$, *APL Mater.*, 2023, **11**, 101128.

30 P. Wang, *et al.*, Ferromagnetic and insulating behavior in both half magnetic levitation and non-levitation LK-99 like samples, *Quantum Front.*, 2023, **2**, 10.

31 Y. Zhang, C. Liu, X. Zhu and H.-H. Wen, Ferromagnetism and insulating behavior with a logarithmic temperature dependence of resistivity in $Pb_{10-x}Cu_x(PO_4)_6 O$, *Sci. China: Phys., Mech. Astron.*, 2023, **67**, 217413.

32 P. K. Jain, Superionic phase transition of copper (I) sulfide and its implication for purported superconductivity of LK-99, *J. Phys. Chem. C*, 2023, **127**, 18253–18255.

33 S. Zhu, W. Wu, Z. Li and J. Luo, First-order transition in LK-99 containing $Cu_2 S$, *Matter*, 2023, **6**, 4401–4407.

34 H. Bai, J. Ye, L. Gao, C. Zeng and W. Liu, Semiconductivity induced by spin-orbit coupling in $Pb_9Cu(PO_4)_6 O$, *Sci. Rep.*, 2023, **13**, 21085.

35 M. W. Swift and J. L. Lyons *Comment on "Origin of correlated isolated flat bands in copper-substituted lead phosphate apatite"*, *arXiv*, 2023, preprint, arXiv:2308.08458.

36 D. Pashov, S. Acharya, S. Lany, D. S. Dessau and M. van Schilfgaarde Multiple slater determinants and strong spin-fluctuations as key ingredients of the electronic structure of electron-and hole-doped $Pb_{10-x}Cu_x(PO_4)_6 O$, *arXiv*, 2023, preprint, arXiv:2308.09900.

37 D. M. Korotin, D. Y. Novoselov, A. O. Shorikov, V. I. Anisimov and A. R. Oganov, Electronic correlations in the ultranarrow energy band compound $Pb_9 Cu(PO_4)_6 O$: A DFT + DMFT study, *Phys. Rev. B*, 2023, **108**, L241111.

38 L. Si, *et al.*, $Pb_{10-x}Cu_x(PO_4)_6 O$: a Mott or charge transfer insulator in need of further doping for (super)conductivity, *J. Phys.: Condens. Matter*, 2023, **36**, 065601.

39 C. Yue, V. Christiansson and P. Werner, Correlated electronic structure of $Pb_{10-x}Cu_x(PO_4)_6 O$, *Phys. Rev. B*, 2023, **108**, L201122.

40 H. Oh and Y.-H. Zhang S-wave pairing in a two-orbital t-J model on triangular lattice: possible application to $Pb_{10-x}Cu_x(PO_4)_6 O$, *arXiv*, 2023, preprint, arXiv:2308.02469.

41 N. Witt, L. Si, J. M. Tomczak, K. Held and T. O. Wehling, No superconductivity in $Pb_9 Cu_1 (PO_4)_6 O$ found in orbital and spin fluctuation exchange calculations, *SciPost Phys.*, 2023, **15**, 197.

42 H. Paudyal, M. E. Flatté and D. Paudyal, Implications of the electron-phonon coupling in $CuPb_9(PO_4)_6 O$ for superconductivity: An ab initio study, *Phys. Rev. Mater.*, 2024, **8**, L011801.

43 S.-W. Kim, *et al.*, On the dynamical stability of copper-doped lead apatite, *npj Comput. Mater.*, 2024, **10**, 16.

44 H. Wang *et al. Observation of diamagnetic strange-metal phase in sulfur-copper codoped lead apatite*, *arXiv*, 2024, preprint, arXiv:2403.11126.

45 Y. Jiang, *et al.*, $Pb_9 Cu(PO_4)_6 (OH)_2$: Phonon bands, localized flat-band magnetism, models, and chemical analysis, *Phys. Rev. B*, 2023, **108**, 235127.

46 J. Cabezas-Escares, *et al.*, Electronic structure and vibrational stability of copper-substituted lead apatite LK-99, *Phys. Rev. B*, 2024, **109**, 144515.

47 K. Haule and G. Kotliar, Coherence-incoherence crossover in the normal state of iron oxypnictides and importance of Hund's rule coupling, *New J. Phys.*, 2009, **11**, 025021.

48 L. de' Medici, J. Mravlje and A. Georges, Janus-faced influence of Hund's rule coupling in strongly correlated materials, *Phys. Rev. Lett.*, 2011, **107**, 256401.

49 A. Georges and L. Medici, d. & Mravlje, J. Strong correlations from Hund-coupling, *Annu. Rev. Condens. Matter Phys.*, 2013, **4**, 137–178.

50 P. Kumar, T. I. Vanhala and P. Törmä, Magnetization, d-wave superconductivity, and non-Fermi-liquid behavior in a crossover from dispersive to flat bands, *Phys. Rev. B*, 2019, **100**, 125141.

51 A. Georges, S. Florens and T. A. Costi, The Mott transition: unconventional transport, spectral weight transfers, and critical behaviour, *J. Phys. IV*, 2004, **114**, 165–173.

52 P. W. Phillips, N. E. Hussey and P. Abbamonte, Stranger than metals, *Science*, 2022, **377**, eabh4273.

53 M.-L. Wang *et al. Unveiling the impact of sulfur doping on copper-substituted lead apatite: A theoretical study*, *arXiv*, 2024, preprint, arXiv:2405.11854.

54 H. Wang *et al. Indications of superconductivities in blend of variant apatite and covellite. arXiv*, 2024, preprint, arXiv:2406.17525.

55 T. Park, *et al.*, Isotropic quantum scattering and unconventional superconductivity, *Nature*, 2008, **456**, 366–368.

56 K. Hashimoto, *et al.*, A sharp peak of the zero-temperature penetration depth at optimal composition in $BaFe_2(As_{1-x}P_x)_2$, *Science*, 2012, **336**, 1554–1557.

57 B. Keimer, S. A. Kivelson, M. R. Norman, S. Uchida and J. Zaanen, From quantum matter to high-temperature superconductivity in copper oxides, *Nature*, 2015, **518**, 179–186.

58 K. Lee, *et al.*, Linear-in-temperature resistivity for optimally superconducting $(Nd,Sr)NiO_2$, *Nature*, 2023, **619**, 288–292.

59 B. Shen, *et al.*, Strange-metal behaviour in a pure ferromagnetic kondo lattice, *Nature*, 2020, **579**, 51–55.

60 P. Blaha, *et al.*, WIEN2k: An APW + lo program for calculating the properties of solids, *J. Chem. Phys.*, 2020, **152**, 074101.

61 J. P. Perdew, K. Burke and M. Ernzerhof, Generalized gradient approximation made simple, *Phys. Rev. Lett.*, 1996, **77**, 3865–3868.

62 K. Haule, Exact double counting in combining the dynamical mean field theory and the density functional theory, *Phys. Rev. Lett.*, 2015, **115**, 196403.

63 K. Haule, C.-H. Yee and K. Kim, Dynamical mean-field theory within the full-potential methods: Electronic structure of ceirin5, cecoin5, and cerhin5, *Phys. Rev. B: Condens. Matter Mater. Phys.*, 2010, **81**, 195107.

64 K. Haule, Quantum monte carlo impurity solver for cluster dynamical mean-field theory and electronic structure calculations with adjustable cluster base, *Phys. Rev. B: Condens. Matter Mater. Phys.*, 2007, **75**, 155113.

65 P. Werner, A. Comanac, L. de' Medici, M. Troyer and A. J. Millis, Continuous-time solver for quantum impurity models, *Phys. Rev. Lett.*, 2006, **97**, 076405.